Journal for ImmunoTherapy of Cancer

Pyroptosis activates conventional type I dendritic cells to mediate the priming of highly functional anticancer T cells

Jordon M Inkol,[1] Michael J Westerveld,[1] Shayla G Verburg,[1] Scott R Walsh,[1] Jodi Morrison,[2] Karen L Mossman,[3] Sarah M Worfolk,[1] Kaslyn LF Kallio,[1] Noah J Phippen,[1] Rebecca Burchett,[4] Yonghong Wan,[4] Jonathan Bramson ,[4] Samuel T Workenhe [1]

To cite: Inkol JM, Westerveld MJ, Verburg SG, *et al*. Pyroptosis activates conventional type I dendritic cells to mediate the priming of highly functional anticancer T cells. *Journal for ImmunoTherapy of Cancer* 2024;**12**:e006781. doi:10.1136/jitc-2023-006781

► Additional supplemental material is published online only. To view, please visit the journal online (https://doi.org/10.1136/jitc-2023-006781).

Accepted 13 March 2024

[1]Department of Pathobiology, University of Guelph, Guelph, Ontario, Canada
[2]Department of Biomedical Sciences, University of Guelph, Guelph, Ontario, Canada
[3]Department of Medicine, McMaster University, Hamilton, Ontario, Canada
[4]Pathology and Molecular Medicine, McMaster University, Hamilton, Ontario, Canada

Correspondence to
Dr Samuel T Workenhe; sworkenh@uoguelph.ca

ABSTRACT

Background Initiation of antitumor immunity is reliant on the stimulation of dendritic cells (DCs) to present tumor antigens to naïve T cells and generate effector T cells that can kill cancer cells. Induction of immunogenic cell death after certain types of cytotoxic anticancer therapies can stimulate T cell-mediated immunity. However, cytotoxic therapies simultaneously activate multiple types of cellular stress and programmed cell death; hence, it remains unknown what types of cancer cell death confer superior antitumor immunity.

Methods Murine cancer cells were engineered to activate apoptotic or pyroptotic cell death after Dox-induced expression of procell death proteins. Cell-free supernatants were collected to measure secreted danger signals, cytokines, and chemokines. Tumors were formed by transplanting engineered tumor cells to specifically activate apoptosis or pyroptosis in established tumors and the magnitude of immune response measured by flow cytometry. Tumor growth was measured using calipers to estimate end point tumor volumes for Kaplan-Meier survival analysis.

Results We demonstrated that, unlike apoptosis, pyroptosis induces an immunostimulatory secretome signature. In established tumors pyroptosis preferentially activated CD103$^+$ and XCR1$^+$ type I conventional DCs (cDC1) along with a higher magnitude and functionality of tumor-specific CD8$^+$ T cells and reduced number of regulatory T cells within the tumor. Depletion of cDC1 or CD4$^+$ and CD8$^+$ T cells ablated the antitumor response leaving mice susceptible to a tumor rechallenge.

Conclusion Our study highlights that distinct types of cell death yield varying immunotherapeutic effect and selective activation of pyroptosis can be used to potentiate multiple aspects of the anticancer immunity cycle.

WHAT IS ALREADY KNOWN ON THIS TOPIC

⇒ Chemoradiotherapies activate the immune response, although the contribution of individual stress and cell death to anticancer immunity remains unknown.

WHAT THIS STUDY ADDS

⇒ This study shows that pyroptosis, unlike apoptosis, is an immunostimulatory type of cell death activating type I conventional dendritic cells to prime durable T cell-mediated antitumor immunity.

HOW THIS STUDY MIGHT AFFECT RESEARCH, PRACTICE OR POLICY

⇒ The implications are pyroptosis inducing agents should be further tested for development as anticancer therapies for patients with cancer.

BACKGROUND

Immunotherapy has demonstrated success in many types of human cancers.[1] However, a few human cancers poorly respond to immunotherapy due to tumor intrinsic barriers of T cell priming and trafficking into the tumor or immunosuppressive microenvironment preventing cytotoxic CD8$^+$ T cells to kill cancer cells.[2] Therefore, there is a need for therapies that can subvert the intratumoral immunosuppression by reigniting the anticancer immunity cycle to elevate the magnitude and functionality of T cells within the tumor.[3]

Chemoradiotherapies render tumors to emit danger signals, cytokines, and chemokines thereby stimulating the anticancer immunity cycle.[3 4] Collectively, these biomolecules regulate the activity of antigen presenting cells as well as the trafficking of cytotoxic T cells into the tumor.[5] Indeed, chemoradiotherapies,[6] photodynamic therapy,[7] oncolytic viruses (OVs),[8–16] and many other immunogenic cell death (ICD) inducers can modify the tumor microenvironment and often facilitate the eradication of established tumors. However, most cytotoxic anticancer treatments simultaneously activate a mixture of premortem stress and programmed cell death. Furthermore, chemotherapies directly impact the quantity and/or functionality of immune cells, complicating the

interpretation of mechanisms contributing to clinical effects and outcomes driven by specific types of cancer cell stress and cell death.

Depending on the type of cytotoxic agent and cellular pathways engaged, during ICD, cancer cells can die by apoptosis,[6] necroptosis,[17] pyroptosis[18] and ferroptosis.[19] In most scenarios, cell death takes place in the background of premortem endoplasmic, oxidative, and mitochondrial stress.[20] As a result, the individual contribution of premortem stress and cell death pathways to anticancer immunity is largely unknown.[21] Anthracycline and oxaliplatin activate apoptosis along with autophagic stress response to emit immunostimulatory secretomes.[22] Expressing procell death proteins to drive specific types of cell death is unraveling immunological outcomes.[23 24] Activation of necroptosis by RIPK3 dimerization, but not apoptosis after caspase 8/9 expression, elicits potent antitumor immunity.[23 24] In the same study, necroptosis driven by RIPK3 lacking RIPK1 interaction domain failed to activate NF-kb mediated inflammation and consequently failed to initiate protective anticancer immunity.[23] In contrast, another study reported terminal cell lysis by expressing mixed lineage kinase domain like pseudokinase (MLKL) mRNA activated potent anticancer immunity.[25] These studies highlight that so much remains unknown about how distinct types of cancer cell death can shape the overall intratumoral immune landscape and anticancer effect.

Pyroptosis is one of the immune-stimulatory cancer cell death modalities and it can be induced by chemotherapy, photodynamic therapy,[18 26] and OVs,[27] cytotoxic $CD8^+$ T cells[28–31] and NK cells.[32] Irrespective of the type of pyroptosis-inducing stimuli and upstream signaling cascade, the cleavage of the gasdermin family of proteins by caspases and granzymes is a terminal event during pyroptosis.[18 33–36]

Enforced expression of full-length gasdermin E protein promotes granzyme mediated pyroptosis initiating T cell-mediated anticancer effect.[28] However, detailed mechanisms by which pyroptosis modifies the tumor microenvironment and how it modulates antigen presentation to prime antitumor T cells remains unknown. Using two murine tumor models, we report that unlike apoptosis, driven by dimerizable (dd) C-terminal caspase-8 (dd-C_{term}-Cas8), pyroptosis, activated by N-terminal gasdermin E (N_{term}Gas) induced a higher amount of calreticulin on the cell surface, emitted danger signals ATP and HMGB1, as well as cytokines and chemokines. These biomolecules potently stimulated conventional dendritic cell (cDC1) and associated expansion and intratumoral recruitment of antigen-specific cytotoxic $CD8^+$ T cells and lower amounts of regulatory T cells within the tumor thereby promoting anticancer effect and extension of the overall survival of tumor-bearing mice.

RESULTS

Pyroptosis emits danger signals and proinflammatory cytokines and chemokines

To define the immunological events and anticancer outcomes after induction of apoptosis and pyroptosis, we developed genetic models of rapid and synchronized cell death by inducibly expressing procell death proteins (figure 1A,D). Doxycycline (Dox) treatment activated the expression of dd-C_{term}-Cas8 (figure 1B) and N_{term}Gas (figure 1E) in mouse colon cancer (MC-38) and lung cancer cells derived from K-ras^{G12D} $p53^{loxP/loxP}$ (KP) mice (KP1.9)[37] (online supplemental file 2). Expression of dd-C_{term}-Cas8 activated apoptosis, as evidenced by cleavage of caspase 3 (figure 1B). In addition, expression of procell death proteins, dd-C_{term}-Cas8 and N_{term}Gas showed reduced cellular metabolism used as a proxy to measure cell viability (figure 1C,F and online supplemental file 2). Pyroptotic but not apoptotic cells showed elevated surface expression of calreticulin (figure 1G) and higher amounts of danger signals HMGB1 (figure 1H), and ATP (figure 1I, online supplemental file 2) in cell-free supernatants. In addition, compared with untreated controls, pyroptotic cells emitted significantly increased amounts of proinflammatory cytokines and chemokines (IL-1β, IL-2, IL-16, IL-9, CXCL9, CX3CL1, and CCL3) and decreased of eotaxin (CCL11) and G-CSF (figure 1J and online supplemental file 3). On the other hand, apoptotic cells emitted higher amounts of cytokines and chemokines (IL-2, IL-9, IL-11, IL-20, IFN-γ, IFN-β, eotaxin, CCL10, CCL21, CCL22) (figure 1J and online supplemental file 4). Cytokines and chemokines downregulated during apoptosis include IL-1a, IL-16, LIF, G-CSF, GMCSF, CCL12, VEGF, CCL5, CCL2, CX3CL1, and KC (figure 1J and online supplemental file 4). In addition to the remarkable differences in the types of cytokine and chemokines emitted, there were notable differences in the kinetics of their secretion. Pyroptosis-induced cytokines and chemokines increased over time from 2 hours to 4 hours. In contrast, most of the cytokine and chemokines emitted during apoptosis showed transient increase at the 2 hour time point and declined by the 4 hour time point (figure 1J).

Established tumors of MC-38-dd-C_{term}-Cas8 or MC-38-N_{term}Gas expressed the procell death proteins after feeding of mice with a Dox-medicated diet (figure 2A,B). Analysis of 44-plex cytokines/chemokines in pyroptotic tumor homogenates showed significant increase in IL-1a, IL-6, IFN-β, IL-16, CXCL2, CCL21, and CCL22 (figure 2C and online supplemental file 5). Furthermore, pyroptotic tumors had decreased levels of cytokines and chemokines associated with protumor macrophages, and myeloid-derived suppressors cells (CCL2, CCL5, M-CSF) (figure 2C and online supplemental file 5). On the other hand, apoptotic tumors showed significantly higher levels of IL-9, IL-4 and CXCL2 and significant downregulation of IL-16, CCL5, IFN-b, LIF, IL-17, GMCSF (figure 2C and online supplemental file 6). Overall pyroptosis induces a profound immune-stimulating cytokine profile in vivo.

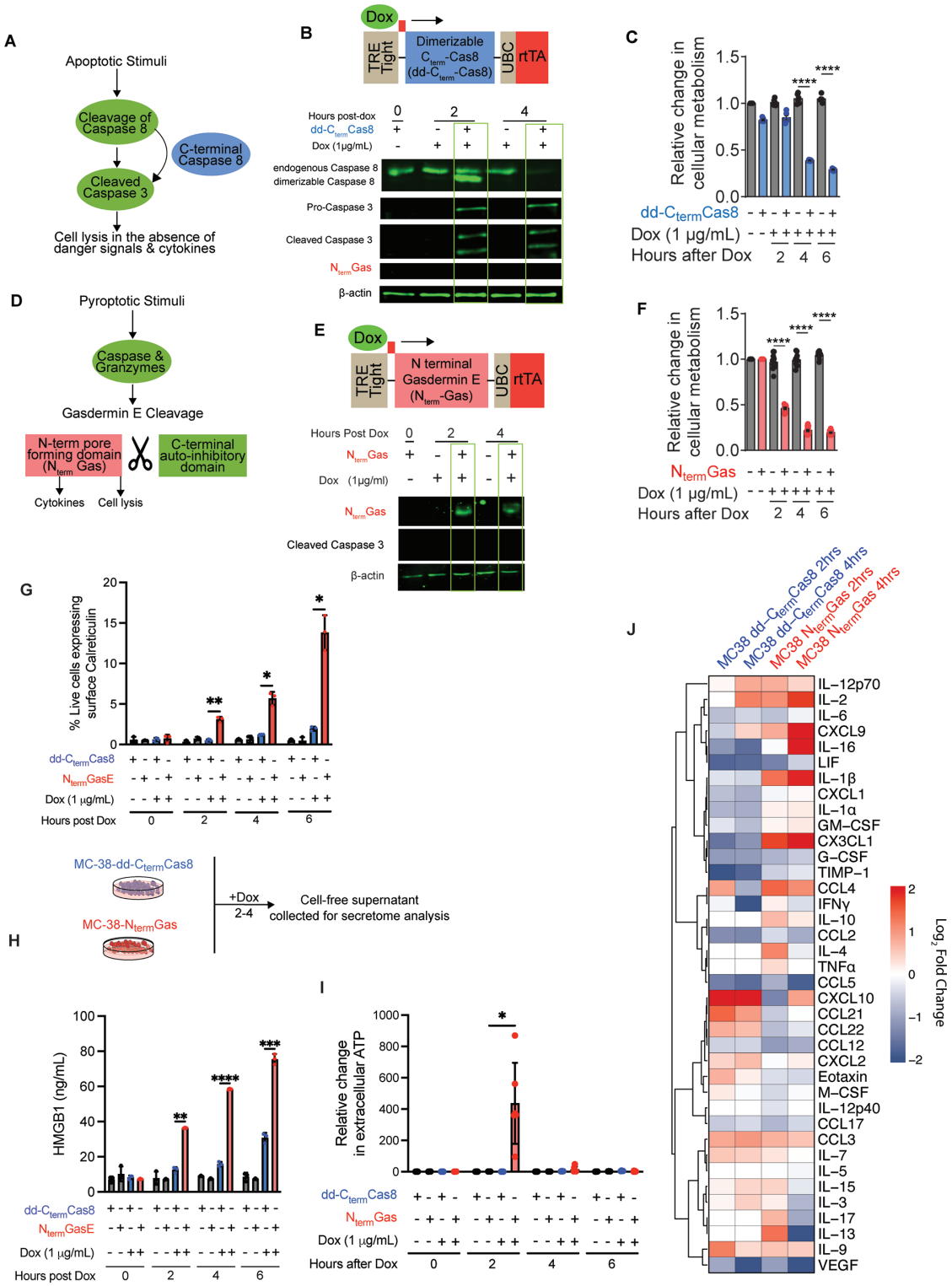

Figure 1 MC-38 cells undergoing pyroptosis express calreticulin on the cell surface and emit higher level of HMGB1 and ATP. (A, D) Schematics of respective apoptosis and pyroptosis effector proteins. (B, E) Immunoblots showing expression of dd-C_{term}Cas8 or N_{term}Gas in Dox-treated MC-38 cells. (C, F) Kinetics of cell viability after inducible expression of N_{term}Gas (N=5) or dd-C_{term}Cas8 (N=5). Error bars, SD. P values were determined using two-way ANOVA with Tukey HSD with significance indicated (****p<0.0001). (G) ELISA showing HMGB1 in cell-free supernatants of pyroptotic cells (N=3). Error bars, SD. P values were determined using two-way ANOVA with Tukey HSD with significance indicated (****p<0.0001, ***p<0.001, **p<0.01). (H) Extracellular ATP secretion at different time points post apoptosis (N=5) and pyroptosis (N=5). Error bars, SD. P values were determined using two-way ANOVA with Tukey HSD with significance indicated (*p<0.083). ((I) Heatmap of Log_2 fold changes of cytokines and chemokines secreted 2 and 4 hours after induction of pyroptosis (N=3) and apoptosis (N=3) compared with baseline at 0 hour for each respective group. Hierarchical clustering distance was defined on Pearson correlation coefficients. ANOVA, analysis of variance; dd, driven by dimerizable; HSD, honest significant difference.

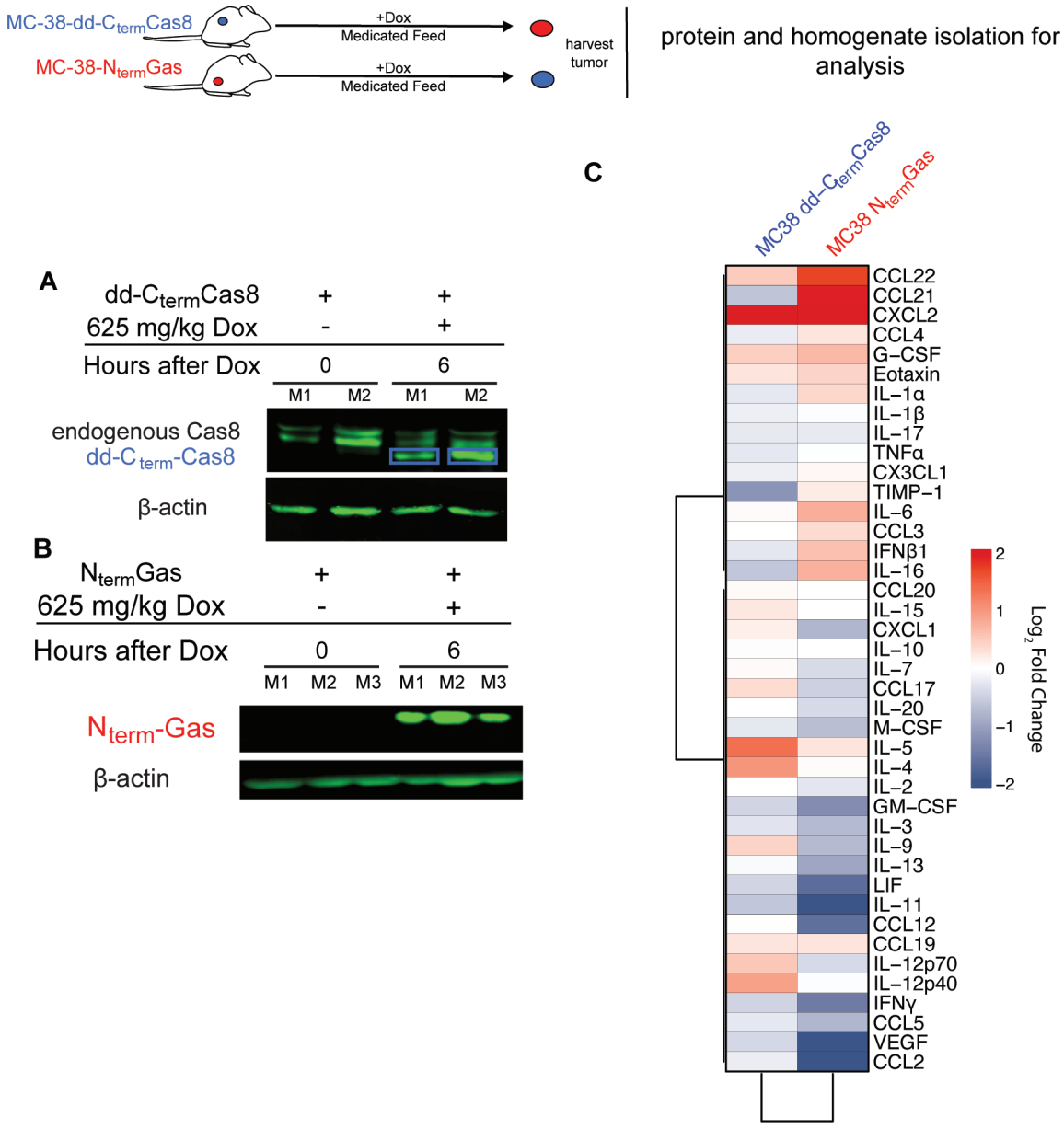

Figure 2 Pyroptotic tumors have an inflammatory cytokine and chemokine signature. (A, B) Immunoblotting of N_{term}Gas (N=3) or C_{term}Cas8 (N=2) in tumor homogenates harvested 6 hours after Dox-medicated diet. (C) Heatmap of log2 fold changes of cytokines and chemokines in pyroptotic (N=5) and apoptotic (N=5) tumor homogenates 24 hours after induction compared with untreated control homogenates of each respective group. Hierarchical clustering distance was defined on Pearson correlation coefficients.

Pyroptosis preferentially activates type I cDCs

To evaluate the immune landscape after cell death, we established chimeric tumors by transplanting a mixture of parental MC-38 along with either MC-38-dd-C_{term}-Cas8 or MC-38-N_{term}Gas cells. Prior to establishing tumors, we confirmed that parental and N_{term}Gas expressing cells have similar in vitro growth kinetics (online supplemental file 7), as a result, transplantation faithfully recapitulated chimeric tumors that activate apoptosis (online supplemental file 8) or pyroptosis after feeding of mice with Dox-medicated diet (online supplemental file 8).

To define the early processes influencing adaptive immunity after induction of cell death we quantified cDC within the tumor and draining lymph nodes (figure 3 and online supplemental file 9). Within the tumor, unlike apoptosis, pyroptosis preferentially induced a 24-hour time peak of cDC1 quantity with a higher phagocytic capacity as evidenced by uptake of ZsGreen expressed in tumors (figure 3A). Moreover, pyroptosis activated cDC1 had expressed SIINFEKL epitope in the context of MHC (figure 3A). Consistent with this, pyroptosis exposed tumors showed elevated cDC1 activation markers including CD40, CD80 and CD86 (figure 3B). Tumor draining lymph nodes showed a delayed but similar pattern of pyroptosis-specific increase in cDC1 quantity, phagocytic activity, antigen presentation and costimulatory molecule expression at the 48-hour time point (figure 3C,D). Both apoptosis

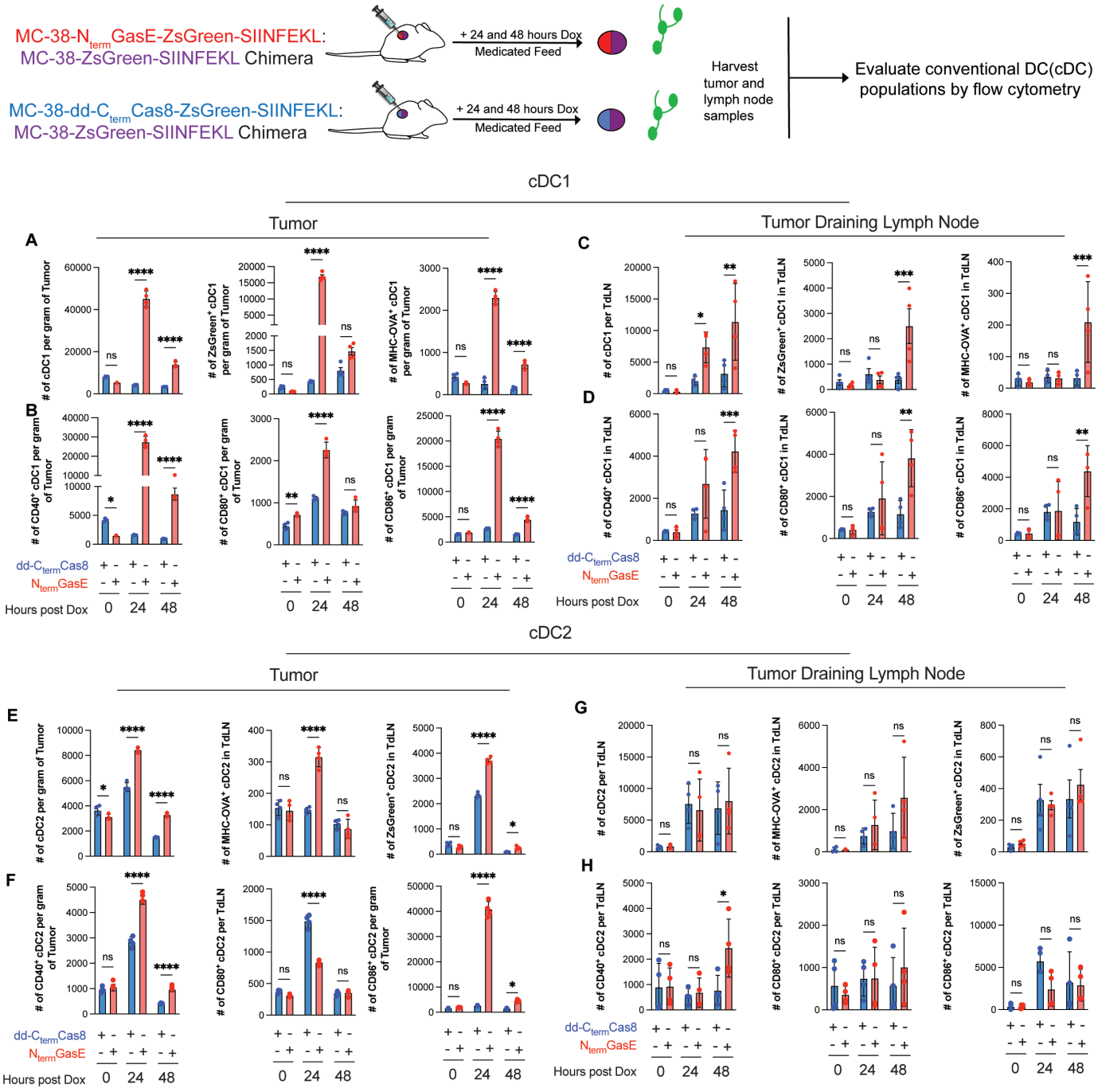

Figure 3 Intratumoral pyroptosis preferentially activates conventional type I dendritic cell (cDC1) in the tumor and draining lymph node. Quantification of total cDC1 within the tumor (N=4) and TdLN (N=4) as well as phagocytic capacity and antigen presentation (A, C). Evaluation of costimulatory marker presence on conventional type I DCs (B, D). Quantification of total cDC2 within the tumor (N=4) and TdLN (N=4) as well as phagocytic capacity and antigen presentation (E, G). Evaluation of costimulatory marker presence on conventional type I DCs (F, H). Error bars, SD. P values were determined using two-way ANOVA with Bonferroni correction with significance indicated. *p <0.05, **p<0.01, ***p<0.001, ****p<0.0001; ANOVA, analysis of variance; ns, not significant.

and pyroptosis increased the total cDC2 count within the tumor, although pyroptosis had significantly higher number (figure 3E). Both types of cell death had intratumoral peak of cDC2 mediated phagocytic activity at the 24-hour time point (figure 3E). However, only pyroptosis exposed cDC2 showed elevated expression of SIINFEKL epitope (figure 3E). Both types of cell death stimulated CD40 expression in cDC2, although apoptosis induced CD80 and pyroptosis preferentially activated CD86 (figure 3F). In the tumor draining lymph node, apoptosis and pyroptosis exposed mice did not show significant difference in cDC2 quantity, phagocytic activity, antigen presentation and costimulatory molecules expression. However, both apoptosis and

pyroptosis exposed mice had a higher cDC2 quantity and phagocytic activity (figure 3G,H).

Tumor-specific CD8+ T cells drive the antitumor response during pyroptosis

We next examined if the cDC1 response generated during pyroptosis translated into tumor specific $CD8^+$ T cell response. For this, we established chimeric tumors expressing the LCMV glycoprotein gp33 epitope. Seven days after start of Dox-medicated diet, we quantified T cell responses in the blood or within the tumor. Pyroptosis generated higher number of tumor infiltrating $CD8^+$ T cells compared with apoptosis that also showed a moderate T cell infiltrate compared with control tumors (figure 4A). Both apoptosis and pyroptosis showed equivalent increase in gp-33 specific $CD8^+$ T cells in the circulation (figure 4B, online supplemental file 10); however, pyroptosis primed antigen experienced $CD44^+$ $CD8^+$ T cells displayed a higher activation pattern as defined by CD69 expression (figure 4C). Consistent with the proportion of activated T cells, pyroptosis primed cytotoxic T cells showed a higher killing capacity against cocultured gp33 expressing MC-38 cells (figure 4D). Restimulation of TILs with a cocktail of peptides (gp33, and MC-38 neoantigens, Adgpk, and Rpl18) followed by intracellular cytokine staining (ICS) revealed only pyroptosis exposed tumors had a higher IL-2^+, TNF-α^+ or concurrent IL-2^+ and TNF-α^+ $CD8^+$ T cells suggestive of polyfunctionality (figure 4E–H, online supplemental file 11). Surprisingly, pyroptosis-induced antigen specific T cells did not secrete IFN-γ (figure 4G). Consistent with highly functional cytotoxic T cells, pyroptosis exposed tumors had a lower quantity of T_{reg} within the tumor (figure 4I).

Pyroptosis extends survival of tumor-bearing mice in cDC1 and T cell-dependent manner

Given the higher magnitude of activated cDC1 and cytotoxic T cell response, we evaluated the antitumor benefits of pyroptosis in prophylactic and therapeutic settings. MC-38-N_{term}Gas and MC-38-dd-C_{term}Cas8 tumor-bearing mice were fed with Dox-medicated diet to eradicate primary tumors within 7 days (figure 5A). Rechallenge of pyroptosis and apoptosis exposed mice with parental MC-38 tumors on the contralateral flank conferred 40% and 85% long-term survival, respectively (figure 5B,C). All the naïve mice challenged with MC-38 tumor cells showed 100% tumor growth. Apoptosis, but not pyroptosis, exposed mice fully succumb to the second tumor rechallenge done at 100 days. In addition, 40% of the pyroptosis exposed mice remained refractory against subsequent rechallenges done at 200 days (figure 5C).

We next examined if the induction of pyroptosis results in therapeutic benefit. Induction of pyroptosis slowed the growth of chimeric tumors (figure 5D) and extended the median survival of mice (median survival of 29 days, 25% of the mice remained tumor-free) compared with apoptosis (median survival of 12 days, no tumor-free mice) (figure 5E). The treatment benefit was consistent in large chimeric MC-38 tumors where induction of pyroptosis displayed extension of median survival (online supplemental file 12, apoptosis having 12 days median survival vs pyroptosis conferring 20 days median survival). The anticancer effects of pyroptosis extends to a non-T cell inflamed KP1.9 tumor model since pyroptosis exposure prolonged the median survival of tumor-bearing mice (median survival of parental tumors—11 days, KP1.9+KP1.9-N_{term}Gas chimeric tumor without Dox-medicated diet- 14 days, KP1.9+KP1.9-N_{term}Gas chimeric tumor fed with Dox-medicated diet—19 days) (online supplemental file 13). Collectively, the findings suggest that in prophylactic and therapeutic settings pyroptosis provides better antitumor immunity than apoptosis.

To determine the antitumor contribution of cDC1, we assessed tumor growth and survival in wildtype versus *Batf3*$^{-/-}$ mice that lack cDC1. While pyroptosis protected 80% of the wildtype mice on tumor rechallenge, *Batf3*$^{-/-}$ mice lacking cDC1 were fully susceptible to tumor rechallenge (figure 6A) even after transfer of wildtype $CD8^+$ T cells (figure 6B). Furthermore, the depletion of $CD8^+$ T cells but not $CD4^+$ (online supplemental file 14) completely ablated the antitumor immune response of pyroptosis rendering mice susceptible to the tumor rechallenge (figure 6C).

Discussion/conclusion

In this study, we elucidated that synchronized and rapid cancer cell apoptosis and pyroptosis have remarkable differences in danger signal, cytokine, and chemokine emission as well as anticancer effect dependent on cDC1 and CD8 T^+ cells.

Our findings that show pyroptosis stimulates anticancer immunity through the release of danger signals and proinflammatory cytokines is in line with results from previous reports.[28 32] Consistent with the role of cDC1 in pyroptosis, we found higher level of chemokines CCL21 and CCL22 in pyroptotic tumor homogenates. It is tempting to speculate these chemokines to be associated with the cDC1-mediated anticancer immunity.[38–40] A recent scRNA seq identified $CCL22^+$ cDC1 population after CD40 agonist therapy in MC-38 tumors.[41] In addition, CCL21 is a CCR7 ligand, and it is crucial for cDC1 trafficking into the draining lymph node. In our study, the contribution of cDC1 during pyroptosis-mediated antitumor immunity was best confirmed using *Batf3*$^{-/-}$ mice where loss of cDC1 completely ablated the antitumor response. Supporting this, pyroptosis exposed tumors and draining lymph nodes are endowed with a higher quantity of cDC1 displaying uptake of dying cancer cells, activation markers and presentation of the antigens in the context of MHC. Previous studies have elucidated that intratumorally injected necroptotic fibroblasts elicit cDC1 dependent antigen presentation and T cell activation.[23] The types of cytokines and chemokines emitted during necroptosis[23] and our tumor pyroptosis are remarkably different and it remains intriguing how distinct ICD-associated secretomes shape cDC1

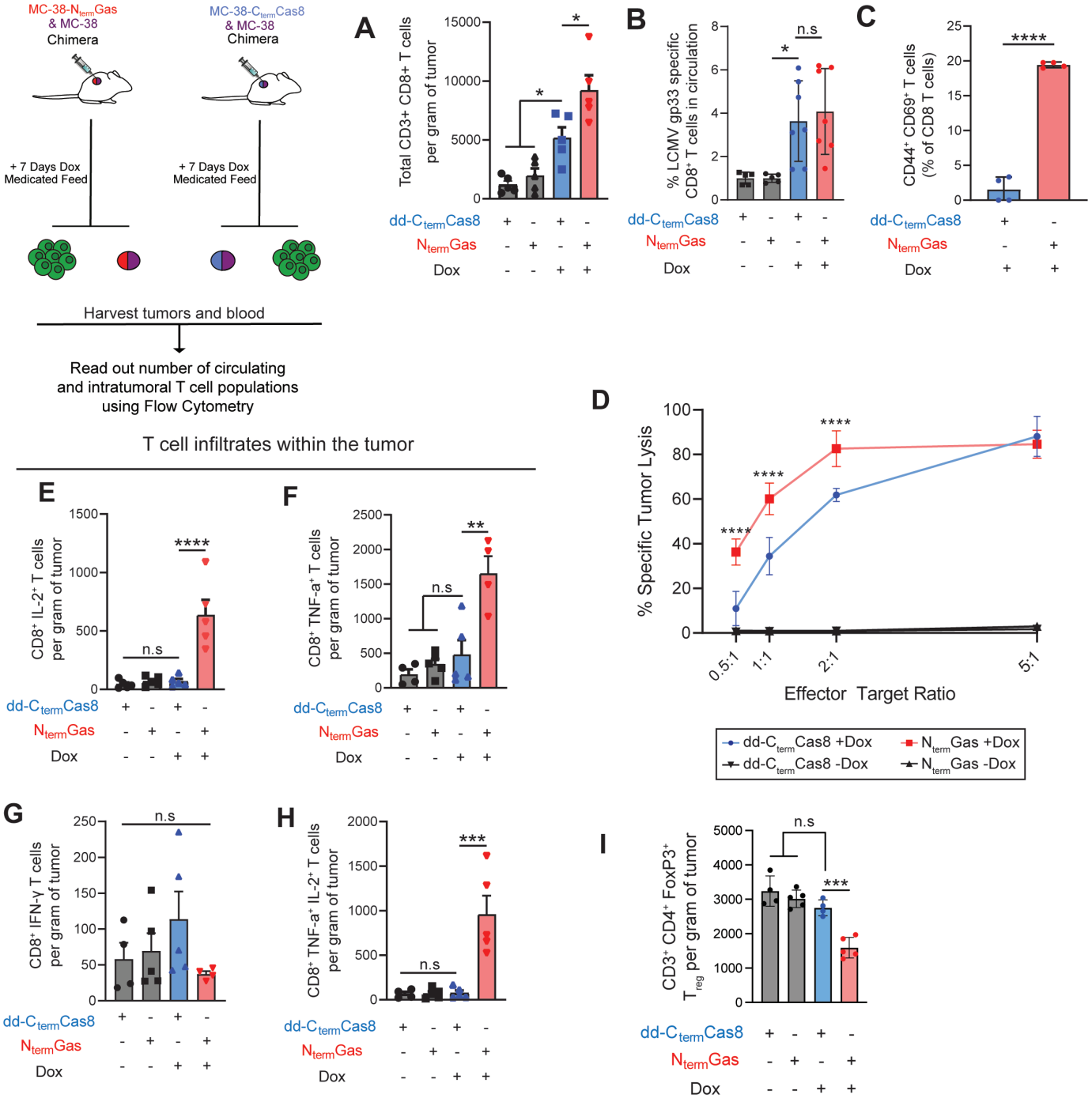

Figure 4 Pyroptosis induces a polyfunctional antitumor antigen agnostic T cell response (A) Quantification of the number of infiltrating CD8⁺ T cells in chimeric tumors 7 days after activation of apoptosis (N=5) or pyroptosis (N=5). Error bars, SD. P values were determined using one-way ANOVA with Bonferroni correction with significance indicated (*p<0.0083). (B) Quantification of the frequency of LCMV-gp33-specific CD8⁺ T cells in circulation after activation of pyroptosis (N=5) or apoptosis (N=5) in chimeric tumors. Errors, SD. P values were determined using one-way ANOVA with Bonferroni correction with significance indicated (*p<0.0083). (C) Pyroptosis elicits significantly higher frequency of antigen experienced CD44⁺ CD69⁺CD8⁺ T cells within the spleen (N=4). Error bars, SD. P values were determined using Student's t test with significance indicated (****p<0.0001). (D) Percent specific lysis of MC-38-gp33 cells after coculture with pyroptosis (N=4) and apoptosis (N=4) stimulated CD8⁺ T cells. Error bars, SD. P values were determined using two-way ANOVA with Tukey HSD with significance indicated (****p<0.0001). (E–H) Analysis of IL-2, TNF-a, IFN-g and IL-2⁺+TNFa⁺ coexpressing CD8⁺ T cells after restimulation with a peptide cocktail (Adgpk and Rpl18 and gp33) (N=5). Error bars, SD. P values were determined using one-way ANOVA with Bonferroni correction with significance indicated (****p<0.0001, ***p<0.0002, **p<0.001). (I) Analysis of CD3⁺CD4⁺ FoxP3⁺ regulatory T cells isolated from apoptosis (N=5) and pyroptosis (N=5) exposed chimeric tumors. Error bars, SD. P values were determined using one-way ANOVA with Bonferroni correction with significance indicated (***p<0.0002). ANOVA, analysis of variance; HSD, honest significant difference.

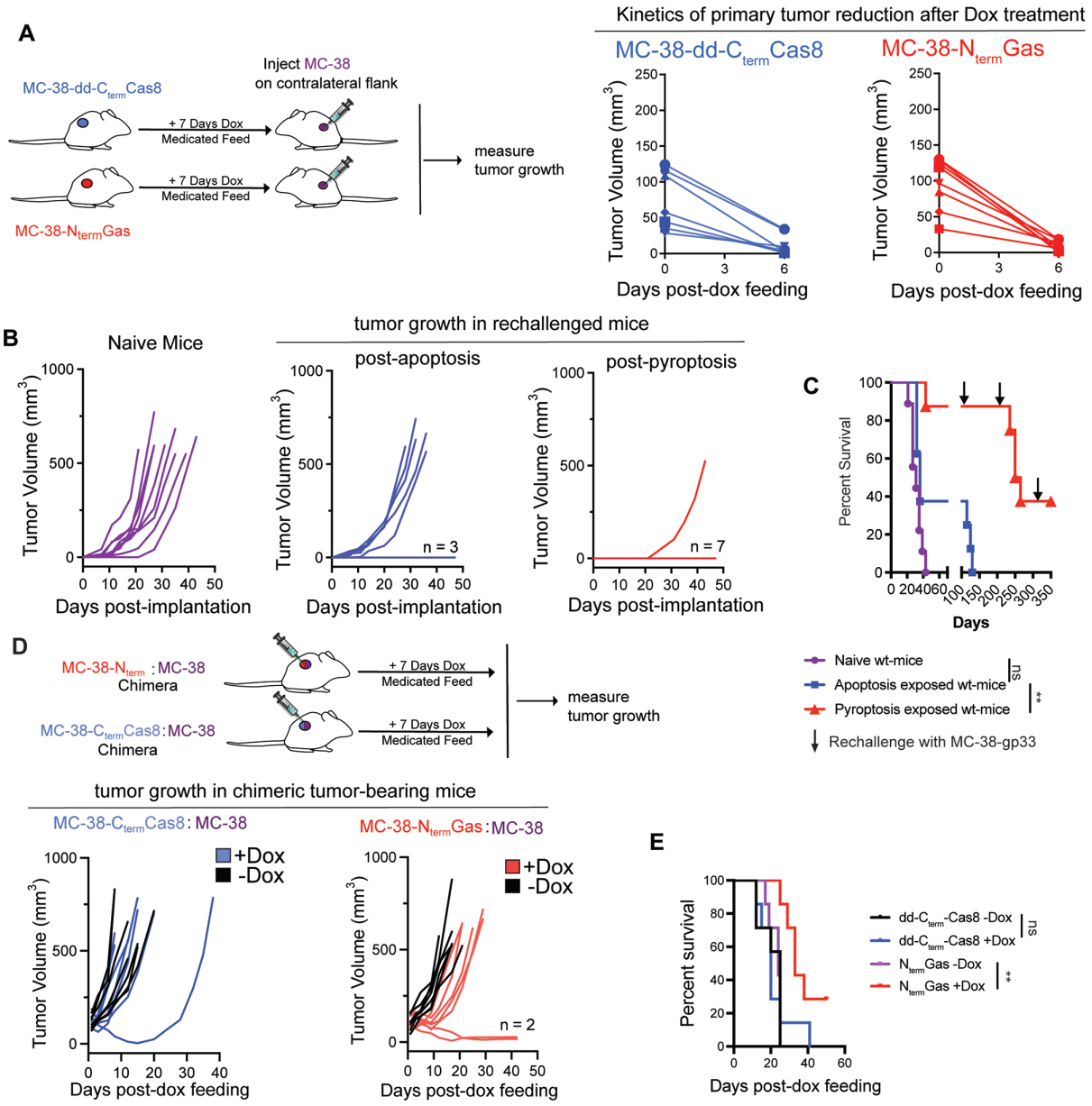

Figure 5 Antitumor immunity generated by pyroptosis confers extended survival of tumor-bearing mice in therapeutic and prophylactic settings (A) Tumor growth kinetics after feeding Dox-medicated diet to MC-38-N_{term}Gas (N=7) or MC-38-dd-C_{term}Cas8 (N=7) tumor bearing mice. (B, C) Overall tumor growth and survival of contralaterally implanted MC38-gp33 tumors in the presence or absence of a prior tumor apoptotic (N=7) or pyroptotic exposure (N=7). P values were determined using log-rank (Mantel-Cox) test with Bonferroni correction with significance set at p<0.016. (D, E) Overall tumor growth and survival of apoptosis (N=7) and pyroptosis (N=7) exposed chimeric tumors. P values were determined using log-rank (Mantel-Cox) with Bonferroni correction with significance set at p<0.016. **p<0.0016.

heterogeneity and functionality. Hence, this model of pyroptosis can be exploited as a ligand-free system to understand numerous aspects of cDC1 biology including chemotaxis factors that facilitate cDC1 trafficking as well as transcriptome changes that dictate the role of cDC1 in antigen uptake and presentation.

Pyroptosis activated a high proportion of circulating and tumor infiltrating cytotoxic T cells (TILs). ICS analysis of TILs after restimulation with the neoantigen peptide cocktail showed secretion of IL-2 and TNF-α but not IFN-γ. In addition, pyroptosis primed cytotoxic T cells isolated from spleen of tumor-bearing mice had a higher proportion of rapidly reactivated antigen experienced $CD44^{+}CD69^{+}$ expressing T cells that exerted robust killing of cocultured tumor cells. Consistent with these qualities of pyroptosis primed T cells, we observed higher protection conferred to pyroptosis, unlike apoptosis, exposed mice at 100 days after the rechallenge. Future studies will investigate if the functionality of pyroptosis primed T cells is mediating the long-term protection against rechallenge. It also remains to be seen if pyroptosis primed T cells can infiltrate non-T cell inflamed tumors and function in highly suppressive tumor microenvironments. At the least, the finding of

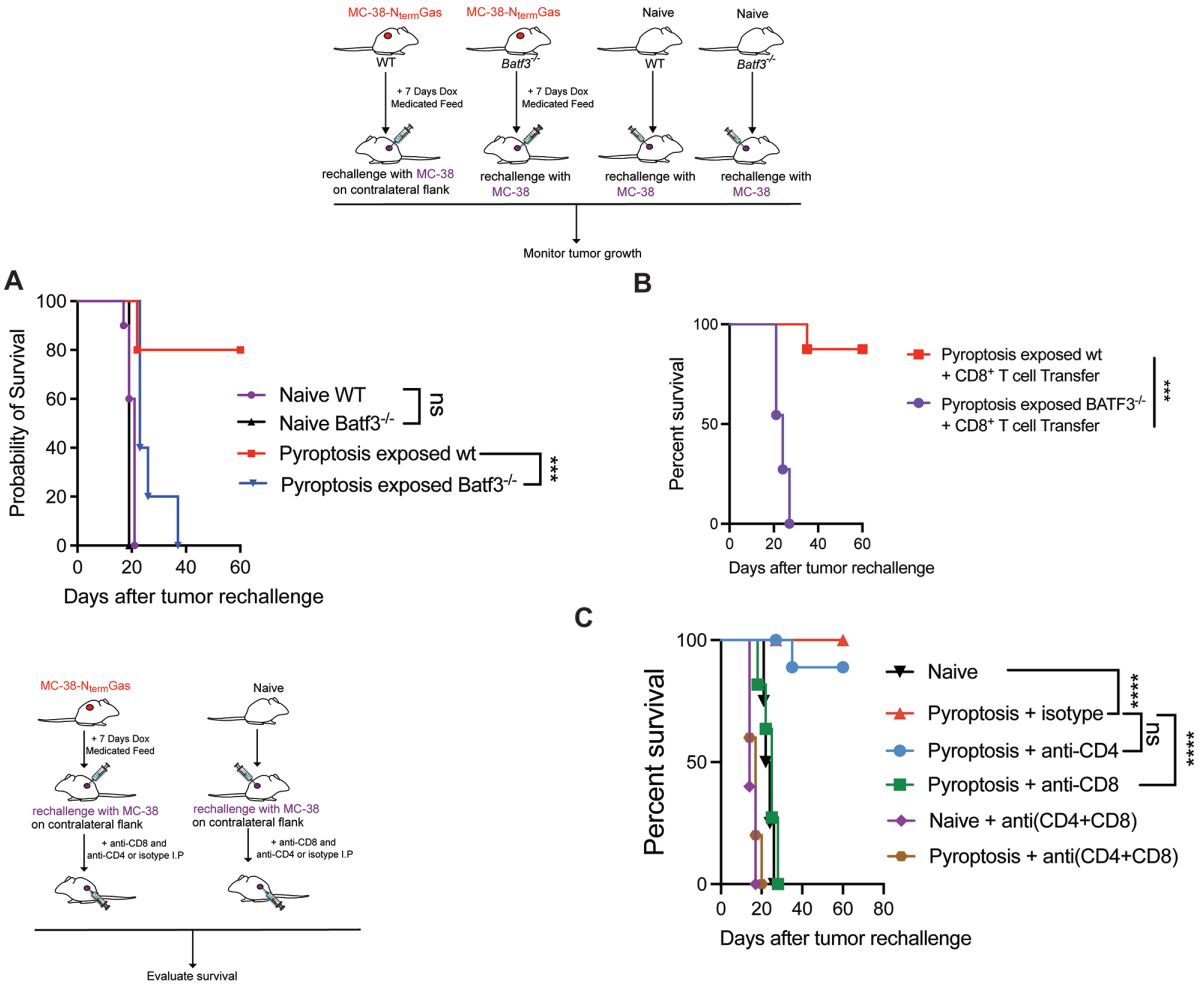

Figure 6 Pyroptosis-induced antitumor immunity is reliant on BATF3$^+$ DCs and T cells (A) Comparison of survival after tumor rechallenge in naïve (N=8) and pyroptosis (N=8) exposed BATF3$^{-/-}$ or wildtype (N=8) C57bl/6 mice. P values were determined using log-rank (Mantel-Cox) test with Bonferroni correction with significance set at p<0.016. (B) Comparison of survival in naïve and BATF3$^{-/-}$ pyroptosis exposed mice after adoptive cell transfer of CD8$^+$ cells. P values were determined using log-rank (Mantel-Cox) test with significance set at p<0.05. (C) Comparison of survival in naïve or pyroptosis exposed mice with or without CD4 (N=7), CD8 (n=8), or CD4 and CD8 (N=8) T cell depletion. P values were calculated using log-rank (Mantel-Cox) test with Bonferroni correction with significance set at p<0.0033. *** p<0.0001; **** p<0.00001. DC, dendritic cell.

reduced T_{reg} in pyroptosis exposed tumors is suggestive of its broader immunostimulatory effects in the tumor microenvironment.

Our findings highlight that pyroptosis provides superior systemic and long-lasting antitumor immunity compared with apoptosis. Hence, approaches to activate cancer cell pyroptosis via pharmacological or genetic methods can be translated into patients with cancer to reignite the anticancer immunity. In fact, some cancers evade immune attack by downregulating the pyroptosis effector gasdermin proteins. Hence, targeted delivery of gasdermin A3 provided potent anticancer effect.[42] In addition, engineered OVs have successfully delivered cell death payloads such as MLKL to induce necroptosis.[43] Lastly, engineered OVs expressing gasdermin or those OVs naturally activating pyroptosis[27] should be rigorously evaluated in humanized mouse settings to evaluate their anticancer effect against patient derived xenografts.

METHODS

Cell culture

Murine colon adenocarcinoma (MC-38) was maintained in Dulbecco's Modified Eagle's media supplemented with 10% fetal bovine serum (FBS) and 100 U/mL of penicillin/streptomycin (P/S). KP 1.9 is a cloned lung adenocarcinoma cell line that arose spontaneously in a K-ras^{LA1}/p53$^{R172H\Delta g}$ mouse model. KP 1.9 cells were a generous gift from Prof. Alfred Zippelius (University Hospital Basel, Switzerland), who originally developed the cell line. KP 1.9 cells were maintained in Iscove Modified Dulbecco media with 10% FBS and 100 U/mL P/S.

Generation of stable N terminus gasdermin E and caspase 8 expressing cell lines

N-terminal gasdermin E (N_{term}Gas) and dimerizable (dd) C-terminal Caspase 8 (dd-C_{term}Cas8) DNA sequences were cloned into the piggyBac (pB) vector (pB-TET) downstream of a Dox inducible TRE-tight promoter

as previously described.[44] MC-38-gp33 and KP-1.9 were transfected using a lipofectamine 3000 (Invitrogen) and the three vector constructs PB-TET-N_{term}Gas or PB-TET-dd-C_{term}Cas8 (response plasmid with cell death protein of interest), PB-CAG-rtTA-Neo (expresses regulatory protein, rtTA), and pCyL43 (plasmid that encodes for transposase) in a ratio of 10:5:2, respectively. Transfected cells were selected using neomycin and clones were screened for inducible expression of procell death proteins. Cell death activating MC-38 cell lines were used to express ZsGreen-SIINFEKL, a fusion protein of the fluorescent protein ZsGreen and SIINFEKL epitope. The expression of ZsGreen-SIINFEKL was normalized between MC-38-dd-C_{term}Cas8 and MC-38-N_{term}Gas cell lines by selection of subclones with equivalent geometric mean fluorescent intensities (online supplemental file 15).

Animal experiments

Female C57/Bl6 mice aged 6–8 weeks old (Charles Rivers Laboratories) were subcutaneously implanted with 2 million tumor cells as described previously.[13–15] For therapeutic settings, chimeric tumors were established by injecting 1×10^6 parental MC-38-gp33 or KP-1.9 cells together with 1×10^6 MC-38-gp33 or KP-1.9 cells with an inducible cell death cassette. 12–14 days after implantation, tumors achieved a treatable tumor volume (80–150 mm^3). Prior to start of treatment mice were randomized among groups to ensure an equal tumor volume across treatments and controls. For all studies requiring inducible expression of procell death proteins mice were fed 625 mg/kg Dox-medicated diet (Envigo Teklad, Madison USA). In prophylactic experiments, mice were rechallenged with 2×10^6 MC-38-gp33 cells injected subcutaneously on the contralateral flank after eradication of the primary tumor. *Batf3*$^{-/-}$ mice were purchased from The Jackson Laboratory. For T cell depletion studies, mice were injected intraperitoneally on day 0, 3, and 7 with either isotype or 250 mg anti-CD4 (clone GK1.5, BioXcell) and anti-CD8 (Clone 2.43, BioXcell). For all experiment groups, tumors were measured every 3–4 days with tumor volumes of 1000 mm^3 classified as endpoint.

Quantification of cell viability

Intracellular ATP was measured using the CellTiter-Glo kit (Promega) as a surrogate marker for cell viability. At stated time point, cells were lysed then following the manufacturer's instructions and luminescence reading measured using the Enspire multimode plate reader (PerkinElmer).

In vitro quantification of extracellular HMGB1, ATP, cytokines, and chemokines

Cell-free supernatant from dying and control cells were harvested after centrifugation of the media at 2000 rpm for 10 min. All samples were immediately frozen at −80°C. Extracellular HMGB1 was quantified using an ELISA kit developed by Shino Test (IBL International). The ELISA was conducted according to the manufacturer's instructions. For extracellular ATP analysis, supernatants were analyzed using an ENLITEN ATP assay kit (Promega) according to manufacturer's instructions. Cell-free supernatants were shipped to Eve Technologies for 44-Plex murine cytokine/chemokine analysis.

Quantification of surface calreticulin expression

Expression of surface calreticulin after apoptosis or pyroptosis was quantified using flow cytometry. Briefly, cells were seeded at a density of 150,000 cells/well in a 6-well plate and allowed to adhere for 16 hours before treatment with Dox for stated time points. Cells were then collected and washed with PBS before staining with Fixable Viability Stain 510 and anti-calreticulin-PE (EPR3924, 1:5000). Data were acquired on BD FACS Canto II and analyzed in FlowJo.

Quantification of cytokines, chemokines, and cell death proteins in tumor homogenates

Tumors were resected from mice and diced into small pieces before being homogenized in tissue extraction solution (50 mM Tris, pH 7.4, 250 mM NaCl, 5 mM EDTA, 2 mM Na_3VO_4, 1 mM NaF, 20 mM $Na_4P_2O_7$, 1 mM b-glycerophosphate, 1% NP-40). Tumors were incubated for 30 min on ice and debris was clarified by three sequential steps of centrifugation at 14,000×rpm for 10 min at 4°C. Tumor homogenates with equal concentration of protein were shipped to Eve Technologies (Calgary, Canada) for 44-Plex murine cytokine/chemokine analysis.

Isolation of immune cells

Tumors were resected and weighed before being placed into RPMI containing Liberase TL Research Grade (250 µg/mL; Roche) and DNase I (1 mg/mL; Sigma-Aldrich). Tumors were minced with scissors and incubated at 37°C for 35 min for enzymatic digestion. Tumor pieces were subsequently crushed against a 70 µm filter to generate a single cell suspension. Cells were washed with PBS containing 2% FBS and 1 mM EDTA. Leucocytes were isolated from each respective single cell suspension using a EasySep Release Mouse Biotin Positive Selection Kit (Stem Cell Technologies) in conjunction with an anti-CD45.2-Biotin (Clone 104) according to the manufacturer's guidelines. Tumor draining lymph nodes were harvested and pressed against a 70 µm filter and rinsed with Hanks Balanced Salt Solution. Blood was collected from the retro-orbital sinus and red blood cells were lysed using ACK buffer (150 mM NH_4Cl, 10 mM $KHCO_3$, and 0.1 mM Na_2EDTA, pH 7.3).

Surface and intracellular staining of immune cells

Leucocytes were incubated with Fc block (anti-CD16/anti-CD32) and stained with fluorescently labeled antibodies and Fixable Viability Stain 510 (BD Biosciences). The following antibodies were obtained from BD Biosciences: anti-CD11c-APC-Cy7 (HL3, 1:200), anti-Ly6C-RB545 (AL-21, 1:100), anti-CD40-BV711 (3/23, 1:100),

anti-CD80-BV650 (16–10A1,1:100), anti-CD86-PE-CF594 (GL1, 1:100), anti-I-A^b-PE (AF6-120, 1:100), anti-CD103-PE-Cy7 (M290, 1:100), anti-CD64-BV786 (X54-5/71, 1:100), anti-CD3-FITC (17A2,1:200), anti-CD8-APC-Cy7 (53–6.7, 1:100), anti-CD44-PE (SB/199, 1:100), anti-CD69-APC (H1.2F3, 1:100), anti-CD4-APC-Cy7 (RM4-5, 1:200), anti-IFN-γ-APC (XMG1.2, 1:100), anti-IL-2-PE (JES6-5H4, 1:100), and anti-TNF-α-BV421 (MP6-XT22, 1:100). The following antibodies were from eBioscience: anti-FOXP3-PE (FJK-16s, 1:100), anti-CD11b-Pacific Blue (M1/70, 1:100), and OVA257-264 (SIINFEKL) peptide bound to H-2Kb Monoclonal Antibody (eBio25-D1.16 (25-D1.16))- PE. Anti-XCR1-BV421 (ZET, 1:100) was purchased from Biolegend. For ICS analysis, leucocytes were stimulated with gp33 (KAVYNFATM), Rpl18 (KILTFDRL), and Adgpk (ASMTNMELM) peptides (Biomer Technologies) (1 µg/mL per peptide) for 4 hours at 37°C. GolgiPlug (BD Biosciences) was added for the last 3 hours of incubation. Cells were stained as above in addition fixation and permeabilization using Cytofix/Cytoperm solution (BD Biosciences). To obtain absolute counts of cells, CountBright Absolute Counting Beads (ThermoFisher Scientific) were added to samples following manufacturer's instructions. Other reagents included the Tetramer H-2D(b)-LCMV-gp33-41-PE from the National Institutes of Health Core facility. Data were acquired on a BD FACSCanto II and a Cytek Northern Lights with downstream analysis completed using FlowJo software.

In vitro cytotoxicity assay

MC-38-gp33 cells were labeled with 3 µM carboxyfluorescein succinimidyl ester (CFSE; BD Biosciences) and seeded in a 96-well plate at 10,000 cells per well and cocultured with $CD8^+$ T cells from the spleen for 10 hours. $CD8^+$ T cells were stained with fixable viability stain 510 (BD Biosciences) and evaluated by flow cytometry. Per cent specific lysis was defined previously as: % specific lysis=100×(%specific cell death−% basal cell death)/100−%basal cell death, where basal cell death is the viability of MC-38-gp33 cells without T cells and specific lysis is the viability of CSFE positive MC-38-gp33 cells.[45]

Immunoblotting

Cells were lysed using radioimmunoprecipitation buffer (10 mM phosphate, 137 mM NaCl, 1% NP-40m 0.5% sodium deoxycholate and 0.1% sodium dodecyl sulfate) supplemented with phosphatase inhibitor cocktail (1.2 mM AEBSF, 13.6 µM bestatin 12.3 µM E-64 112 µM leupeptin1.16 µM pepstatin) and protease inhibitor cocktail (Millipore Sigma, Massachusetts, USA). For measuring HMGB1 cell-free supernatants were used. Total protein extracted from cells or tumor homogenates and cell-free supernatants were resolved using 7.5%–15% sodium dodecyl sulfate polyacrylamide gel electrophoresis and transferred to nitrocellulose membranes. Membranes were blocked in Intercept^R (TBS) Blocking Buffer (Li-Cor Biosciences) followed by incubation with primary antibodies. The following antibodies were purchased from Cell Signalling Technologies: anti-Gasdermin E (Cat#40618, 1:3000), anti-β-actin (Cat#4967, 1:6000), and anti-Cleaved-Caspase-3 (Cat#9661, 1:3000). The following antibodies were purchased from Abcam: anti-Caspase-8 (Cat#ab25901, 1:3000). Membranes were then probed with secondary antibody conjugated to an infrared dye (IRDye 800CW Donkey anti-Rabbit IgG, 1:6000) and analyzed using an Odyssey DLx scanner (Li-Cor Biosciences).

Immunohistochemistry

Treated and control tumors were excised from euthanized mice and fixed in 10% formalin for 48 hours and then transferred to 70% ethanol before being embedded into paraffin blocks. Five µm thick tumor sections were deparaffinized prior to incubation in citrate buffer at 95°C for 15 min. Tumor sections were blocked with Intercept^R (TBS) Blocking buffer (Li-Cor Biosciences) before addition of primary antibody. Anti-Gasdermin E (Cell Signalling Technologies, 40618) was diluted in Intercept Blocking Buffer with 0.2% Tween-20 and used at a working dilution of 1:500. Primary antibody was incubated overnight in a humidified chamber at 4°C in the dark. Signal amplification was completed using an anti-rabbit secondary antibody conjugated to Alexa-488 (Abcam, ab150077, 1:10,000). Secondary antibody incubation was performed at room temperature in a humidified chamber in the dark for 2 hours. Sections were counterstained with diluted DAPI (Abcam) for 5 min at room temperature in the dark. Slides were rinsed with MiliQ water before imaging with the Leica DMLB fluorescent.

Statistics and reproducibility

For each statistical test used, normality of the distribution and equality of variance between groups was evaluated beforehand. For differences in means, one-way analysis of variance (ANOVA), two-way ANOVA, Student's two-tailed unpaired t-test, and non-parametric Kruskal-Wallis test were used. The Holm Šidák method was used to correct multiple comparisons. For analyzing differences between experimental groups in Kaplan-Meier survival, the log-rank (Mantel-Cox) test was used with 525 mm^3 as endpoints. Bar graphs are shown as mean±SD. The null hypothesis was rejected for $p<0.05$. All statistical tests and analyses were carried out using GraphPad Prism V.9.

X Jordon M Inkol @always_jord, Michael J Westerveld @MikeWesterveld1 and Samuel T Workenhe @samworkenhe

Acknowledgements We thank the University of Guelph Centralized and Isolation Animal Facility staff for help with animal studies.

Contributors JMI and STW conducted most of the experiments presented in the paper together with MJW, SGV, SRW, SW, KK, NP and JM. MJW and SRW helped with in vivo experiments involving immune cell analysis. SGV, SW, KK and NP conducted ATP, HMGB1 and calreticulin quantification and immunoblotting experiments. JM helped with the tissue section and staining studies. KM financially supported the preliminary in vitro experiments of this study when STW was a postdoctoral fellow in her lab. RB, YW and JB provided p14 splenocytes. JMI and

STW prepared the figures and wrote the manuscript. STW conceived, supervised, and is the guarantor for the study.

Funding STW is funded by Canadian Institute of Health Research (PJT 185868 and PJT 190071), SickKids New Investigator award (NI23-1064R), Cancer Research Society (ID# 942502 and 1056603), Ontario Institute for Cancer Research funding from The Joseph and Wolf Lebovic Cancer Genomics and Immunity Program.

Competing interests None declared.

Patient consent for publication Not applicable.

Ethics approval Mice were maintained at the University of Guelph Isolation Facility and all procedures were completed in compliance with the Canadian Council on Animal Care and approved by the University of Guelph Animal Care Committee (Animal Utilization Protocol (AUP) # 4487).

Provenance and peer review Not commissioned; externally peer reviewed.

Data availability statement Data sharing not applicable as no datasets generated and/or analyzed for this study.

ORCID iDs
Jonathan Bramson http://orcid.org/0000-0003-2874-6886
Samuel T Workenhe http://orcid.org/0000-0001-9521-3903

REFERENCES

1 Wolchok JD, Kluger H, Callahan MK, *et al*. Nivolumab plus Ipilimumab in advanced melanoma. *N Engl J Med* 2013;369:122–33.
2 Lim M, Xia Y, Bettegowda C, *et al*. Current state of immunotherapy for glioblastoma. *Nat Rev Clin Oncol* 2018;15:422–42.
3 Workenhe ST, Pol J, Kroemer G. Tumor-intrinsic determinants of immunogenic cell death modalities. *Oncoimmunology* 2021;10:1893466.
4 Workenhe ST, Inkol JM, Westerveld MJ, *et al*. Determinants for antitumor and protumor effects of programmed cell death. *Cancer Immunol Res* 2024;12:7–16.
5 Kroemer G, Galluzzi L, Kepp O, *et al*. Immunogenic cell death in cancer therapy. *Annu Rev Immunol* 2013;31:51–72.
6 Casares N, Pequignot MO, Tesniere A, *et al*. Caspase-dependent immunogenicity of doxorubicin-induced tumor cell death. *J Exp Med* 2005;202:1691–701.
7 Agostinis P, Berg K, Cengel KA, *et al*. Photodynamic therapy of cancer: an update. *CA Cancer J Clin* 2011;61:250–81.
8 Cuddington BP, Dyer AL, Workenhe ST, *et al*. Oncolytic bovine herpesvirus type 1 infects and kills breast tumor cells and breast cancer-initiating cells irrespective of tumor subtype. *Cancer Gene Ther* 2013;20:282–9.
9 van Vloten JP, Workenhe ST, Wootton SK, *et al*. Critical interactions between immunogenic cancer cell death, oncolytic viruses, and the immune system define the rational design of combination immunotherapies. *J Immunol* 2018;200:450–8.
10 Verburg SG, Lelievre RM, Westerveld MJ, *et al*. Viral-mediated activation and inhibition of programmed cell death. *PLOS Pathog* 2022;18:e1010718.
11 Workenhe ST, Mossman KL. Oncolytic virotherapy and immunogenic cancer cell death: sharpening the sword for improved cancer treatment strategies. *Mol Ther* 2014;22:251–6.
12 Workenhe ST, Mossman KL. Rewiring cancer cell death to enhance oncolytic VIRO-immunotherapy. *Oncoimmunology* 2013;2:e27138.
13 Workenhe ST, Nguyen A, Bakhshinyan D, *et al*. De novo Necroptosis creates an inflammatory environment mediating tumor susceptibility to immune checkpoint inhibitors. *Commun Biol* 2020;3:645.
14 Workenhe ST, Pol JG, Lichty BD, *et al*. Combining oncolytic HSV-1 with immunogenic cell death-inducing drug mitoxantrone breaks cancer immune tolerance and improves therapeutic efficacy. *Cancer Immunol Res* 2013;1:309–19.
15 Workenhe ST, Simmons G, Pol JG, *et al*. Immunogenic HSV mediated oncolysis shapes the antitumor immune response and contributes to therapeutic efficacy. *Mol Ther* 2014;22:123–31.
16 Workenhe ST, Verschoor ML, Mossman KL. The role of oncolytic virus immunotherapies to subvert cancer immune evasion. *Future Oncol* 2015;11:675–89.
17 Yang H, Ma Y, Chen G, *et al*. Contribution of RIP3 and MLKL to immunogenic cell death signaling in cancer chemotherapy. *Oncoimmunology* 2016;5:e1149673.
18 Wang Y, Gao W, Shi X, *et al*. Chemotherapy drugs induce pyroptosis through caspase-3 cleavage of a gasdermin. *Nature* 2017;547:99–103.
19 Efimova I, Catanzaro E, Van der Meeren L, *et al*. Vaccination with early ferroptotic cancer cells induces efficient antitumor immunity. *J Immunother Cancer* 2020;8:e001369.
20 Galluzzi L, Buqué A, Kepp O, *et al*. Immunogenic cell death in cancer and infectious disease. *Nat Rev Immunol* 2017;17:97–111.
21 Kepp O, Kroemer G. Is Ferroptosis immunogenic? The devil is in the details *Oncoimmunology* 2022;11:2127273.
22 Michaud M, Martins I, Sukkurwala AQ, *et al*. Autophagy-dependent anticancer immune responses induced by chemotherapeutic agents in mice. *Science* 2011;334:1573–7.
23 Snyder AG, Hubbard NW, Messmer MN, *et al*. Intratumoral activation of the necroptotic pathway components RIPK1 and RIPK3 potentiates antitumor immunity. *Sci Immunol* 2019;4:36.
24 Yatim N, Jusforgues-Saklani H, Orozco S, *et al*. RIPK1 and NF-KB signaling in dying cells determines cross-priming of $CD8^+$ T cells. *Science* 2015;350:328–34.
25 Van Hoecke L, Van Lint S, Roose K, *et al*. Treatment with mRNA coding for the necroptosis mediator MLKL induces antitumor immunity directed against neo-epitopes. *Nat Commun* 2018;9:3417.
26 Li L, Song D, Qi L, *et al*. Photodynamic therapy induces human esophageal carcinoma cell pyroptosis by targeting the PKM2/caspase-8/caspase-3/GSDME axis. *Cancer Lett* 2021;520:143–59.
27 Lin J, Sun S, Zhao K, *et al*. Oncolytic parapoxvirus induces gasdermin E-mediated pyroptosis and activates antitumor immunity. *Nat Commun* 2023;14.
28 Zhang Z, Zhang Y, Xia S, *et al*. Gasdermin E suppresses tumour growth by activating anti-tumour immunity. *Nature* 2020;579:415–20.
29 Liu Y, Fang Y, Chen X, *et al*. Gasdermin E–mediated target cell pyroptosis by CAR T cells triggers cytokine release syndrome. *Sci Immunol* 2020;5:eaax7969.
30 Minute L, Teijeira A, Sanchez-Paulete AR, *et al*. Cellular cytotoxicity is a form of immunogenic cell death. *J Immunother Cancer* 2020;8:e000325.
31 Jaime-Sanchez P, Uranga-Murillo I, Aguilo N, *et al*. Cell death induced by cytotoxic CD8(+) T cells is Immunogenic and primes caspase-3-dependent spread immunity against endogenous tumor antigens. *J Immunother Cancer* 2020;8:e000528.
32 Zhou Z, He H, Wang K, *et al*. Granzyme a from cytotoxic lymphocytes cleaves GSDMB to trigger pyroptosis in target cells. *Science* 2020;368:eaaz7548.
33 Man SM, Karki R, Kanneganti T-D. Molecular mechanisms and functions of pyroptosis, inflammatory caspases and inflammasomes in infectious diseases. *Immunol Rev* 2017;277:61–75.
34 Rogers C, Alnemri ES. Gasdermins: novel mitochondrial pore-forming proteins. *Mol Cell Oncol* 2019;6:e1621501.
35 Rogers C, Erkes DA, Nardone A, *et al*. Gasdermin pores permeabilize mitochondria to augment caspase-3 activation during apoptosis and inflammasome activation. *Nat Commun* 2019;10:1689.
36 Shi J, Zhao Y, Wang K, *et al*. Cleavage of GSDMD by inflammatory caspases determines pyroptotic cell death. *Nature* 2015;526:660–5.
37 Pfirschke C, Engblom C, Rickelt S, *et al*. Immunogenic chemotherapy sensitizes tumors to checkpoint blockade therapy. *Immunity* 2016;44:343–54.
38 Roberts EW, Broz ML, Binnewies M, *et al*. Critical role for $CD103^+$/$CD141^+$ dendritic cells bearing CCR7 for tumor antigen trafficking and priming of T cell immunity in melanoma. *Cancer Cell* 2016;30:324–36.
39 Salmon H, Idoyaga J, Rahman A, *et al*. Expansion and activation of CD103(+) dendritic cell progenitors at the tumor site enhances tumor responses to therapeutic PD-L1 and BRAF inhibition. *Immunity* 2016;44:924–38.
40 Comerford I, Harata-Lee Y, Bunting MD, *et al*. A myriad of functions and complex regulation of the CCR7/CCL19/CCL21 chemokine axis in the adaptive immune system. *Cytokine Growth Factor Rev* 2013;24:269–83.

41 Zhang L, Li Z, Skrzypczynska KM, *et al*. Single-cell analyses inform mechanisms of myeloid-targeted therapies in colon cancer. *Cell* 2020;181:442–59.
42 Wang Q, Wang Y, Ding J, *et al*. A bioorthogonal system reveals antitumour immune function of pyroptosis. *Nature* 2020;579:421–6.
43 Van Hoecke L, Riederer S, Saelens X, *et al*. Recombinant viruses delivering the necroptosis mediator MLKL induce a potent antitumor immunity in mice. *Oncoimmunology* 2020;9:1802968.
44 Baid K, Nellimarla S, Huynh A, *et al*. Direct binding and internalization of diverse extracellular nucleic acid species through the collagenous domain of class a scavenger receptors. *Immunol Cell Biol* 2018;96:922–34.
45 Walsh SR, Simovic B, Chen L, *et al*. Endogenous T cells prevent tumor immune escape following adoptive T cell therapy. *J Clin Invest* 2019;129:5400–10.